ACS OMEGA

http://pubs.acs.org/journal/acsodf

Article

Dual-Emission Ratiometric Fluorescent Probe Based on Lanthanide-Functionalized Carbon Quantum Dots for White Light Emission and Chemical Sensing

Ying Li,* Ya-Qi Wang, Dan Liu, Yu Gao, Sai-Nan Wang, and Hanxun Qiu

Cite This: *ACS Omega* 2021, 6, 14629−14638

Read Online

ACCESS | Metrics & More | Article Recommendations | Supporting Information

ABSTRACT: Herein, we develop a novel method to synthesize lanthanide-functionalized carbon quantum dots via free-radical copolymerization using the methyl methacrylate (MMA) monomer as a functional monomer and introducing a lanthanide complex to obtain the dual-emission fluorescent composite material FCQDs-Ln$(TFA)_3$ (Ln = Eu, Tb; TFA: trifluoroacetylacetone). The obtained composites were fully characterized, and their structures were investigated by Fourier transform infrared spectroscopy (FTIR), ^{1}H NMR spectroscopy, X-ray photoelectron spectroscopy (XPS), and transmission electron microscopy (TEM). Subsequently, a series of white-light-emitting polymer composite films FCQDs- (Eu:Tb)$(TFA)_3$/poly(methyl methacrylate) (PMMA) were designed and synthesized by adjusting the ratio of Eu$(TFA)_3$/Tb$(TFA)_3$ under different wavelengths. More significantly, FCQDs-Tb$(TFA)_3$ was selected as a sensitive probe for sensing metal cations due to excellent photoluminescence properties, revealing a unique capability of FCQDs-Tb$(TFA)_3$ of detecting Fe(III) cations with high efficiency and selectivity. Furthermore, the sensing experiment results indicated that FCQDs-Tb$(TFA)_3$ is ideal as a fluorescent nanoprobe for Fe^{3+} ion detection, and the lowest detection limit for Fe^{3+} is 0.158 μM, which is superior to many other previous related research studies. This pioneering work provides a new idea and method for constructing a dual-emission ratio sensor based on carbon quantum dots and also extends the potential application in the biological and environmental fields.

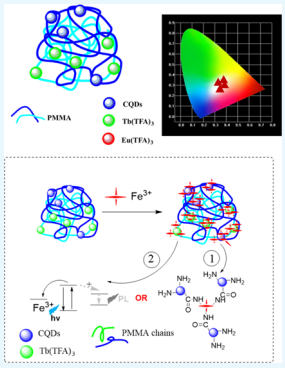

1. INTRODUCTION

The emerging types of carbon fluorescent nanodots have gained increasing attention in recent years.[1−6] Especially, due to the tunable photoluminescence (PL) and specific binding capabilities for specific analytes, some functionalized carbon nanomaterials are considered useful in a wide range of applications, including fluorescent field probes and sensors,[7,8] batteries,[9,10] photocatalysis,[11] biomarkers and medical imaging,[12−14] and light-emitting diode (LED) color displays and lighting.[15,16] These materials with common optical properties include carbon quantum dots (CQDs), carbon nanodots (CND), graphene quantum dots (GQDs), and nanofibers.[17] CQDs are a class of quasispherical nanodots with quantum confinement effects and crystal structures, whose fluorescence is mainly dependent on particle size and excitation wavelength.[18−20] Compared with the traditional semiconductor quantum dots,[21] CQDS have broad development potential due to low toxicity, good biocompatibility, and tunable photoluminescence.[22−25]

It is well known that lanthanides are critical for a variety of advanced optical materials and technologies since they cover various emission spectra of the ultraviolet (UV)−visible and near-infrared (NIR) regions. In a trivalent lanthanide ion, the emission bands of Nd^{3+}, Yb^{3+}, Er^{3+}, and Ho^{3+} are located in the NIR emission region, while Eu^{3+} ions (red light) and Tb^{3+} ions (green light) are located in the visible light emission region, which is visible to the naked eye.[26−28] However, lanthanide complexes have been excluded from practical applications to date considering their relatively low chemical, optical, and thermal stability. Therefore, lanthanide complexes can be used to combine with CQDs because of the functional groups on the surface of CQDs, such as carboxyl groups and amino groups. In addition, water-soluble CQDs can complement the hydrophobicity of lanthanide complexes, which facilitates optical bioimaging.[29] Considering that both lanthanide complexes and carbon quantum dots are fragile and difficult to process, it is necessary to select an appropriate matrix to impart good mechanical toughness and processability to the system.[23] Polymeric materials are suitable substrates for luminescent materials due to good transparency, excellent mechanical strength, good flexibility, cost-effectiveness, and easy to process.[30] Most importantly, making the carbon quantum dots and lanthanides uniformly dispersed in the polymer matrix to fully release the potential of the emitter is a basic prerequisite for the construction of a white fluorescent

Received: March 31, 2021
Accepted: May 13, 2021
Published: May 27, 2021

Scheme 1. Experimental Process and Schematic Diagram of FCQDs-Ln(TFA)$_3$

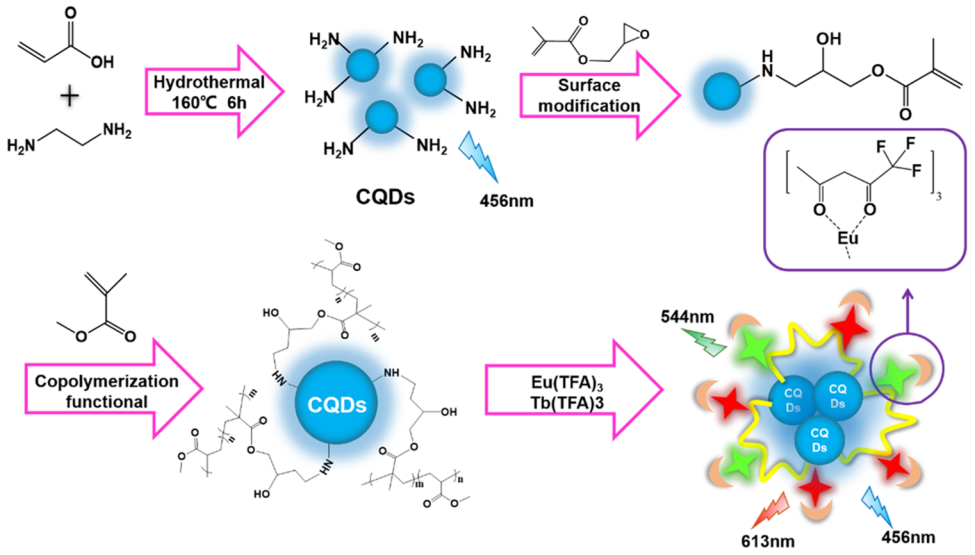

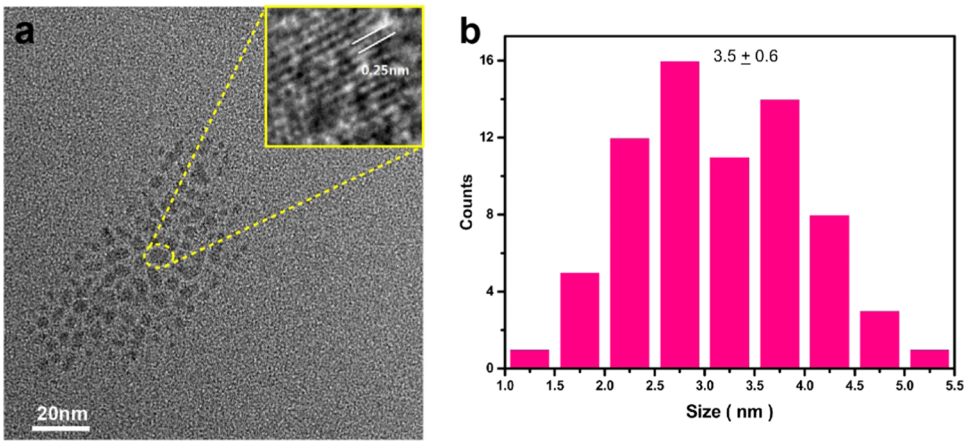

Figure 1. TEM image (a) and particle size distribution of CQDs (b).

emission system. In addition, the dual-emission fluorescent composite material based on the ratio of lanthanide-functionalized carbon quantum dots can not only improve its sensitivity but also avoid the interference of the detection background. Therefore, it is more interesting to explore the application of quantum dots in proportional dual-emission fluorescence. CQD fluorescence sensing has been applied to detect various substances and quantities by monitoring changes in their fluorescence intensity under external physical or chemical stimuli,[31−41] including signal changes caused by concentration fluctuations, optical path lengths, and source intensity, which can interfere with accurate and quantitative measurements.[42] Especially, the great importance of Fe^{3+} in biological and environmental systems has aroused widespread interest in the development of selective techniques for the determination of Fe^{3+} in recent years. Meanwhile, it is urgent and valuable to develop novel fluorescent probes for Fe^{3+} ions with low cytotoxicity, excellent biocompatibility, and high water solubility. Moreover, the functionalized CQDs also displayed the sensing properties, owing to the interaction with metal ions. However, it is rarely reported to design lanthanide complex-functionalized CQDs with strong fluorescence properties through simple synthesis methods and apply them to the field of chemical sensing.

Based on the above considerations, in this work, we developed a novel method to design MMA-functionalized carbon quantum dot (FCQDs) and further introduced lanthanide complexes with fluorescence characteristics into FCQDs via chemical bonds to obtain the dual-emission fluorescent composite material FCQDs-Ln(TFA)$_3$ (Ln = Eu, Tb; TFA: trifluoroacetylacetone). (Scheme 1). FCQDs-Ln(TFA)$_3$ has both the fluorescence emission peak of CQDs and the characteristic fluorescence of Ln^{3+} ions under a specific excitation wavelength, according to the basic requirements of ratiometric fluorescent probes. Moreover, a series of white fluorescent polymer films FCQDs-(Eu:Tb)(TFA)$_3$/poly-(methyl methacrylate) (PMMA) were prepared by taking CQDs as a blue light source and adjusting the ratio of the lanthanide complex with different proportions into the PMMA matrix. The intense white light emission could be observed with the optimum molar ratio (Eu/Tb = 3:7) when excited with a 320 nm laser. The fluorescence characteristics of FCQDs-Tb(TFA)$_3$ and its sensing application to metal cations are explored to realize its high sensitivity and selectivity detection of common metal cations. The results showed that FCQDs-Tb(TFA)$_3$ could be used as a dual-ratio emission fluorescent probe for the specific and sensitive detection of

https://doi.org/10.1021/acsomega.1c01745
ACS Omega 2021, 6, 14629−14638

Fe^{3+} through the quenching of luminescence. In addition, a possible sensing mechanism was also further proposed.

2. RESULTS AND DISCUSSION

2.1. Structural Characterization of CQDs, PCQDs, and FCQDs. The structure and morphology of the CQDs were confirmed by Fourier transform infrared spectroscopy (FTIR), high-resolution transmission electron microscopy (HRTEM), and X-ray photoelectron spectroscopy (XPS) analyses. Figure 1a shows a typical TEM image of the CQDs, which obviously reveals well-dispersed CQD nanoparticles with an average size of 2.0−4.5 nm in diameter. Furthermore, a typical HRTEM image of CQDs indicated that the CQDs have a certain crystal structure with an average lattice spacing of about 0.25 nm and there is no obvious aggregation. (Figure 1b) Such small nanoparticles could effectively minimize the steric hindrance effect and thus make them ideal for the copolymerization to obtain PCQD monomers and FCQDs (see Scheme 1). To better study the structure and surface functional groups of carbon quantum dots, the successful formation of CQDs was further verified by the XPS spectra shown in Figure S1. It can be seen from the XPS spectra that the as-prepared CQDs were mainly composed of three elements C, N, and O, displaying three characteristic peaks corresponding to C 1s (284.8 eV), N 1s (398.5 eV), O 1s (532.5 eV). The high-resolution C 1s spectrum of the CQDs shows signals from C−C/C═C (284.8 eV), C−N (285.4 eV), C−O (286.0 eV), and COOH (289.9 eV), confirming the surface groups of CQDs. (Figure S1B) As shown in Figure S1C, vibration signals of N−H (398.5 eV), N−C═O (400.5 eV), and C−N (401.5 eV) can be observed from the XPS N 1s spectrum of CQDs. In addition, the O 1s spectrum of CQDs is enlarged in Figure S1D. There are three peaks at 531.5, 532.5, and 535.2 eV, representing C═O, C−O, and O═C−O, respectively. By combining the XPS and FTIR spectra (Figure 2), the existence of the functional groups of the

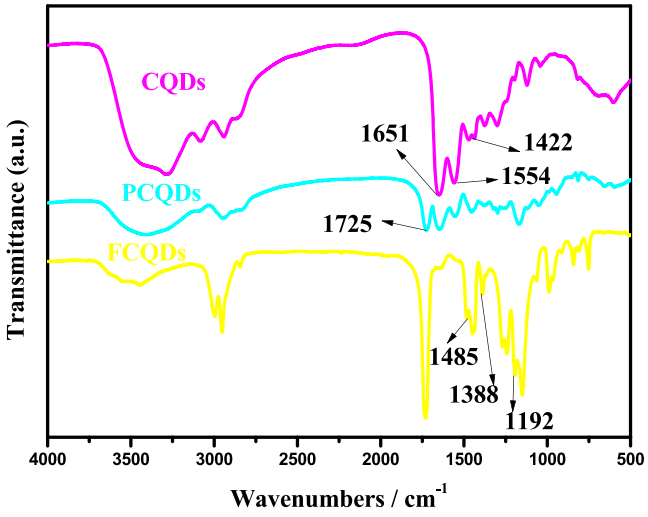

Figure 2. FTIR spectra of CQDs, PCQDs, and FCQDs.

as-prepared CQDs can be speculated. These results indicate that the surface of CQDs is rich enough to be modified by the nitrogen-containing and oxygen-containing groups.

The chemical bonds and functional groups on the CQDs and PCQDs were further characterized by FTIR spectroscopy and ^{1}H NMR spectra. The peaks at 1651, 1554, and 1422 cm^{-1} can be observed from the FTIR spectra of CQDs, which are attributed to the tensile vibrations of C═O, N−H, and C−N, respectively, confirming the formation of the amide bond. (Figure 2) In addition, the O−H and N−H stretching vibration peaks located at about 3000−3500 cm^{-1} also indicate the existence of carboxyl and amino active groups and their bonding methods in CQDs. Meanwhile, the carbonyl peak in PCQDs disappeared and a new band at 1725 cm^{-1} (COOR) indicated that the glycidyl methacrylate (GMA) molecule was successfully modified on the surface of carbon quantum dots to form the polymerizable vinyl group. This is consistent with the ^{1}H NMR spectrum analysis of CQDs and PCQDs (Figure S2). Compared with the pure CQDs, the chemical shifts at δ 6.15 and δ 5.73 (−C═CH_2) in the PCQD spectrum are attributed to the terminal vinyl group of GMA, indicating that the GMA molecule has been successfully connected onto the surface of CQDs. Moreover, the copolymerization of the FCQDs was carried out by reacting PCQDs with the methyl methacrylate (MMA) monomer. (Scheme 1) As expected, the three vibration peaks at 1485, 1388, and 1192 cm^{-1} in the FTIR spectrum are attributed to the stretching vibration of −CH, indicating that the formation of FCQDs by free-radical polymerization. Meanwhile, the double peaks of vinyl hydrogen (−C═CH_2) in the FCQD spectrum disappeared with the newly appeared ^{1}H NMR vibration peak of −CH_2− (δ 1.88) and the chemical shift shifted to the low field, indicating that the monomers were all involved in the polymerization. The reaction confirmed that the MMA monomer and PCQDs were successfully polymerized to obtain FCQDs, which is conducive to the next step of the preparation and performance research of dual-emission fluorescent composite materials.

2.2. Photoluminescence Analysis of CQDs and FCQDs-Ln(TFA)$_3$. The photoluminescence performance is essential to the application of CQDs. As can be seen in Figure 3A, the CQD aqueous solution shows strong blue emission with an obvious peak at 465 nm under an excitation wavelength of 376 nm. The systematic PL emission spectra of the CQD aqueous solution were obtained at different excitation wavelengths ranging from 300 to 480 nm (Figure 3B). The as-synthesized CQDs have typical wavelength-dependent fluorescence emission behaviors at different excitation wavelengths, revealing the red shift phenomenon with the increased wavelength, most probably due to the different surface states and size dispersion of CQDs.[44] Furthermore, the UV−visible spectrum of CQDs is given in Figure S3. It can be observed that CQDs have an almost closed light absorption band in the UV region near 300 nm, which corresponds to the n−π^* transition of C═O. Taking quinine sulfate as a reference, the quantum yield of CQDs reached 71.6% at an excitation wavelength of 380 nm, displaying excellent fluorescence performance.

Compared with CQDs, we measured the fluorescence spectra of composite materials FCQDs-Eu(TFA)$_3$ (A) and FCQDs-Tb(TFA)$_3$ (B) at an excitation wavelength λ_{ex} = 365 nm, as shown in Figure 4. It can be obviously seen from the emission spectra that FCQDs-Ln(TFA)$_3$ (Ln = Eu, Tb) has displayed the dual fluorescence emission under the same excitation wavelength, containing the blue emission of CQDs at 410 nm and the characteristic emission peaks of Ln^{3+}. Figure 4A shows the emission spectrum of FCQDs-Eu(TFA)$_3$, including the maximum peak intensities at 578, 591, 613, and 651 nm, which are attributed to $^5D_0 \rightarrow {}^7F_J$ (J = 0, 1, 2, 3) transitions of Eu^{3+} ions, respectively, with the hypersensitive transition of $^5D_0 \rightarrow {}^7F_2$ as the most prominent line. As shown

https://doi.org/10.1021/acsomega.1c01745
ACS Omega 2021, 6, 14629−14638

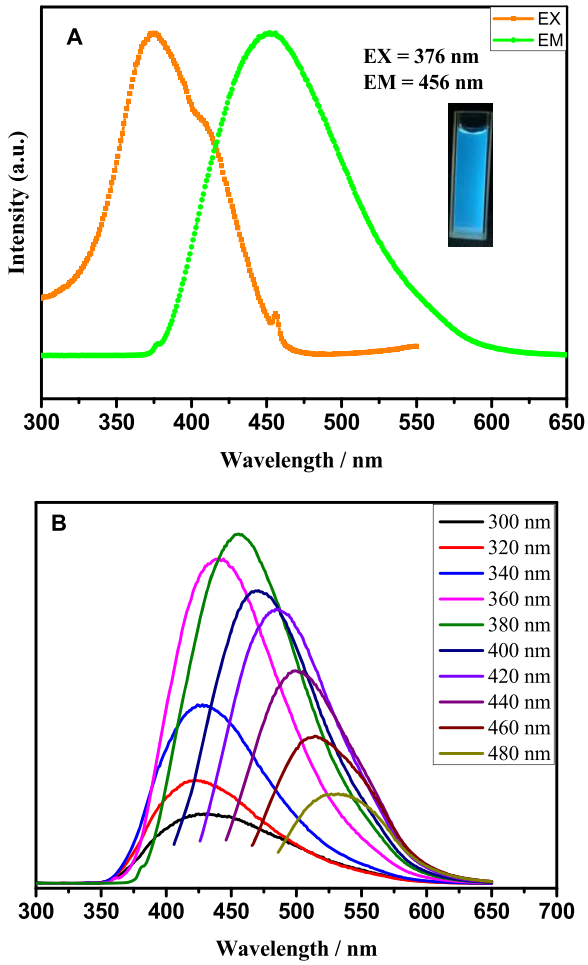

Figure 3. (A) PL emission spectrum of an aqueous solution of the CQDs (λ_{ex} = 376 nm). (B) PL emission spectra of the CQD aqueous solution under different excitation wavelengths.

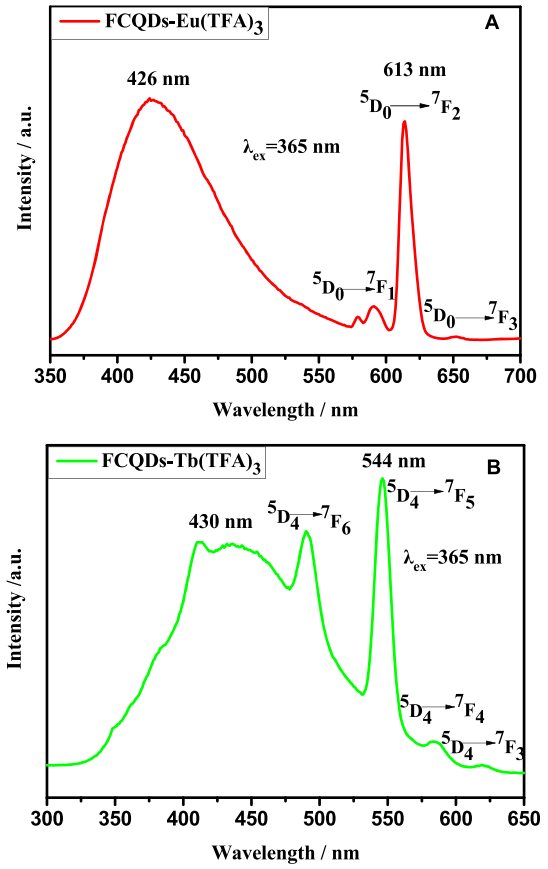

Figure 4. PL emission spectra of FCQDs-Eu(TFA)$_3$ (A) and FCQDs-Tb(TFA)$_3$ (B).

in Figure 4B, the dominant green emission peak of Tb^{3+} of FCQDs-Tb(TFA)$_3$ is at 545 nm ($^5D_4 \rightarrow {}^7F_2$). In addition, to further study the fluorescence stability of the sample, FCQDs-Tb(TFA)$_3$ was chosen as an example to perform the fluorescence test after 1 week of storage (Figure S4). The results show that the fluorescence emission intensity remains basically unchanged, also confirming the fluorescence stability of FCQDs-Tb(TFA)$_3$.

2.3. Sensing Applications of Metal Ions. Due to the vital roles in biological and environmental applications, it is highly necessary to detect trace transition metal ions. Iron is one of the most significant metals in biological systems as well as from an environmental viewpoint. Fe^{3+} plays an important role in many physiochemical processes and biological systems. But when its metabolism is disordered, it can cause anemia, liver and kidney damage, diabetes, and heart failure.[43] Herein, using lanthanide complex-functionalized carbon quantum dots FCQDs-Tb(TFA)$_3$, a fluorescence sensor with dual-emission peaks of CQDs and lanthanide ions was designed for the detection of Fe^{3+}. The influence of various metal cations on the fluorescence intensity of FCQDs-Tb(TFA)$_3$ was investigated by comparing the fluorescence intensity in the presence of a series of metal cations (Pb^{2+}, Cd^{2+}, Mg^{2+}, Zn^{2+}, Co^{3+}, Ni^{+}, K^{+}, Mn^{2+}, Cu^{2+}, Ca^{2+}, Fe^{2+}, and Fe^{3+}) under a λ_{ex} of 365 nm. As shown in Figure 5a, the fluorescence intensity of FCQDs-Tb(TFA)$_3$ significantly decreased in the presence of Fe^{3+}, while the other ions exhibit weak or even negligible effects on their fluorescence intensities. Furthermore, Figure 5b displays the relative intensities of $^5D_4 \rightarrow {}^7F_5$ at 545 nm for FCQDs-Tb(TFA)$_3$ dispersed in the aqueous solutions of different metal ions (10^{-3} mol/L) when excited at 365 nm. Fe^{3+} displays the most obvious quenching effect on the PL intensity of FCQDs-Tb(TFA)$_3$, as compared with the other metal ions. These results indicate that FCQDs-Tb(TFA)$_3$ shows a selective response to Fe^{3+} and therefore could be utilized as a nanosensing platform for Fe^{3+} detection.

For better sensitivity studies on the fluorescence response of FCQDs-Tb(TFA)$_3$ to Fe^{3+}, different concentrations of Fe^{3+} were added to the aqueous solutions containing the same amount of FCQDs-Tb(TFA)$_3$ to evaluate the detection ability of Fe^{3+}. As shown in Figure 6a, the fluorescence emission peaks of the CQDs and Tb^{3+} decreased significantly with the increase of Fe^{3+} concentration from 0 to 1000 μM. The double fluorescence peak almost completely disappeared when the Fe^{3+} concentration reached 1000 μM, suggesting that FCQDs-Tb(TFA)$_3$ is sensitive to Fe^{3+}. In addition, the fluorescence response of FCQDs-Tb(TFA)$_3$ toward Fe^{3+} was linear in a concentration range of 0−500 μM (Figure 6b), and the quenching effect can be rationalized quantitatively by the Stern−Volmer equation as follows[45]

$$I_0/I = 1 + K_{SV}[M]$$

where I_0 and I are the luminescent intensities of FCQDs-Tb(TFA)$_3$ at 365 nm before and after the introduction of the Fe^{3+} solution, respectively. K_{SV} is the coefficient of quenching, and [M] represents the concentration of Fe^{3+}. According to the

https://doi.org/10.1021/acsomega.1c01745
ACS Omega 2021, 6, 14629−14638

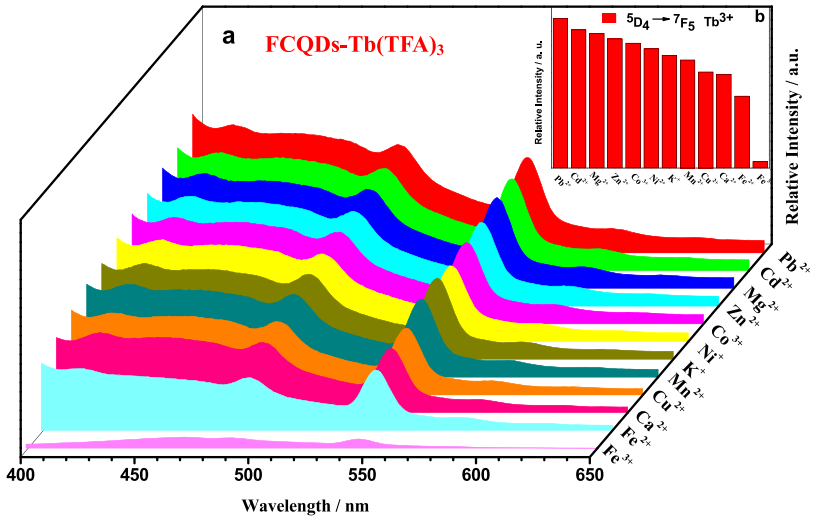

Figure 5. (a) Emission spectrum and (b) the relative intensities of $^5D_4 \rightarrow {}^7F_5$ at 545 nm for FCQDs-Tb(TFA)$_3$ dispersed in the aqueous solutions of different metal ions (10^{-3} mol/L) when excited at 365 nm.

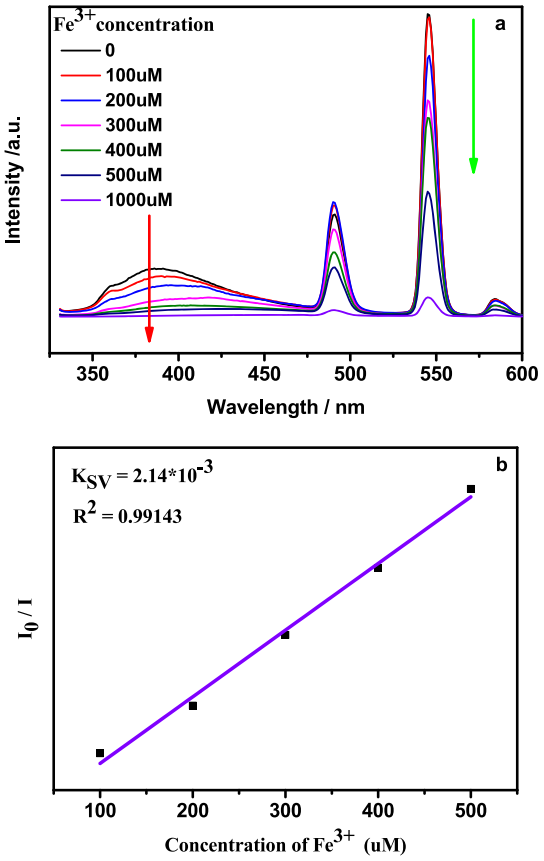

Figure 6. (a) PL intensity of FCQDs-Tb(TFA)$_3$ as a function of Fe^{3+} concentration in aqueous solution. (b) The plot of I_0/I versus the concentration of Fe^{3+}.

data in Figure 6b, K_{SV} is fitted to be 2.14×10^{-3} with a good linear correlation (R^2 = 0.99143), which indicates that the quenching effect of Fe^{3+} on CQDs-Tb(TFA)$_3$ is according to the Stern−Volmer model. The lowest detection limit (LOD) is also calculated to be 0.157 μM based on the three times the standard deviation rule according to the formula

$$\mathrm{LOD} = 3\delta/S$$

where δ is the standard deviation of the blank signal and S is the slope of the linear calibration graph. Compared with the previously reported Fe^{3+} sensor based on CQDs (Table 1), the

Table 1. Comparison of the Sensing Performance of Different Fluorescent Probes for Fe^{3+} Detection

methods	linear range (μM)	LOD	ref
lignin-derived CQDs	0−350	0.196 μM	47
CDs (ammonium citrate)	0−20	0.87 μM	48
sulfur-doped CDs	0−872	0.56 μM	49
CDs (citric acid and ethylenediamine)	0−1000	0.239 μM	50
CDs (vitamin B1)	0−330	0.177 μM	51
S-doped C-dots	0−500	0.1 μM	52
N, Zn-CDs	0.05−125	0.027 μM	53
FNCDs	2.0−25	0.9 μM	54
CQDs-Tb(TFA)$_3$	0−50	0.158 μM	this work

dual-emission fluorescent composite CQDs-Tb(TFA)$_3$ has a superior detection limit and sensitivity for Fe^{3+} sensing. The above results confirm that the FCQDs-Tb(TFA)$_3$ composite can be used as a fluorescent nanosensor with high detection of Fe^{3+} in an aqueous environment.

Furthermore, the photostability of FCQDs-Tb(TFA)$_3$ was investigated under different pH values, as demonstrated in Figure S5. By adjusting the pH of the solution, the fluorescence response of the FCQDs-Tb(TFA)$_3$ aqueous solution is measured in Figure S5A,B. It can be observed that the fluorescence intensities of the FCQDs-Tb(TFA)$_3$ composite material first gradually increases and then slowly decreases in a pH range of 2−12. Especially, it exhibits the strongest fluorescence at pH = 7. It is worth noting that the two emission peaks of FCQDs-Tb(TFA)$_3$ display completely the opposite fluorescence responses under excitation at 365 nm, which is just in accordance with the characteristics of a ratiometric fluorescence sensor. Figure 7 shows the linear relationship between I_{545}/I_{405} and pH, which can also clearly express that the FCQDs-Tb(TFA)$_3$ composite has the strongest fluorescence in a neutral aqueous solution,

https://doi.org/10.1021/acsomega.1c01745
ACS Omega 2021, 6, 14629−14638

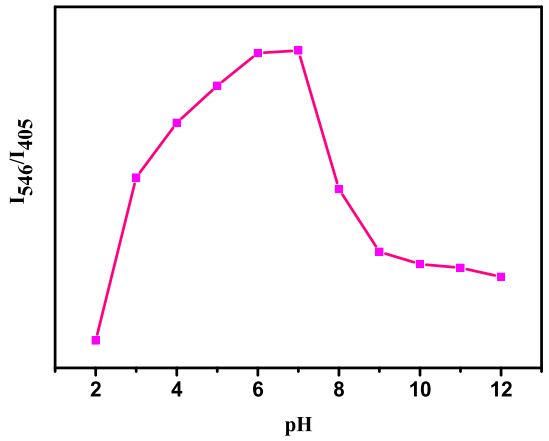

Figure 7. Photostability of FCQDs-Tb$(TFA)_3$ under different pH values.

confirming that the FCQDs-Tb$(TFA)_3$ dual-emission composite materials can be used as pH fluorescent nanosensors.

The possible reaction mechanism of FCQDs-Tb$(TFA)_3$ in the presence of Fe^{3+} ions is speculated as follows (Figure 8):

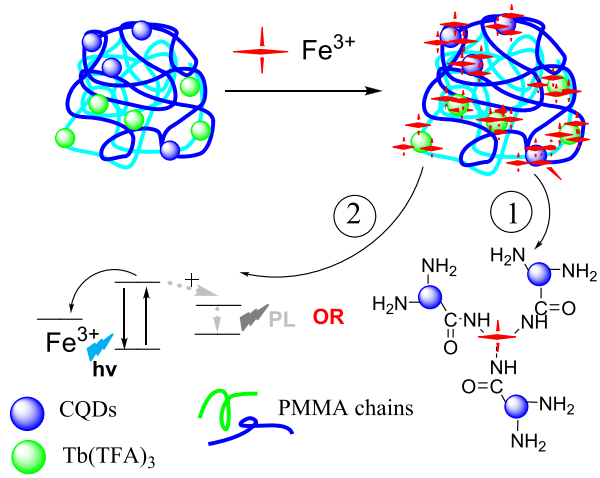

Figure 8. Mechanism of fluorescence quenching of Fe^{3+} ions.

On the one hand, the surface of FCQDs-Tb$(TFA)_3$ contains a large number of amide bonds (−CONH−) that can interact with Fe^{3+} ions to form complexes. The electronic structure of CQDs and the distribution of excitons can be affected by the chemical bond. This process allows the charge- or energy-transfer process to promote the nonradiative recombination of excitons and results in the transfer of the excited electrons from the surface of CQDs to the half-filled 3d orbitals of Fe^{3+} ions, which leads to obvious fluorescence quenching.[46] On the other hand, the competitive absorption may generate between Fe^{3+} ions and the unsaturated lanthanide complex Tb$(TFA)_3$, causing a hindrance in the energy transfer between the lanthanide ions and the ligand, thereby reducing the fluorescence intensity.

2.4. White Photoluminescence Tuning Properties of the Film. Considering that CQDs and two kinds of lanthanide ions (Eu^{3+} and Tb^{3+}) exhibit the primary colors (blue, red, and green), it is expected that we can obtain the white polymer thin film FCQDs-(Eu:Tb)$(TFA)_3$/PMMA. Comparing the ultraviolet−visible (UV−vis) spectra of Tb$(TFA)_3$ and FCQDs-(Eu:Tb) $(TFA)_3$/PMMA, it can be clearly seen that the FCQDs-(Eu:Tb)$(TFA)_3$/PMMA film shows broad absorption in a wavelength range of 260−290 nm, but the peak is blue-shifted by about 18 nm (274 → 292 nm; Figure S6). This is attributed to the charge transfer from $n \rightarrow \pi^*$ to $n \rightarrow \sigma^*$ after the carbonyl oxygen atom coordinated with the Tb^{3+} ion in FCQDs, which further confirmed that the FCQDs formed coordination bonds with lanthanide ions. It can also be observed from the inset photos that the FCQDs-(Eu:Tb)-$(TFA)_3$/PMMA film is transparent and free of impurities, indicating that CQDs and lanthanide complexes can be uniformly dispersed in the PMMA matrix. In addition, the PMMA chain can also be used as the macromolecular ligand of the unsaturated lanthanide complex during the preparation of the film to promote the uniform dispersion of Ln^{3+} ions and FCQDs.

The emission spectrum of the film FCQDs-(Eu:Tb)-$(TFA)_3$/PMMA shows three main peaks at λ_{ex} = 300 nm (Figure 9A) and λ_{ex} = 320 nm (Figure 9 B), which correspond to the emission peak of CQDs (368 nm) and the characteristic peaks of Ln^{3+} (Tb^{3+}: 545 nm and Eu^{3+}: 613 nm), respectively. Furthermore, the CIE chromaticity coordinates can also be found in the white light region. It can obviously be observed from the figure that when the ratios of Eu$(TFA)_3$/Tb$(TFA)_3$ are 4:6, 3:7, and 2:8, the composite film is in the white light region under excitation of 300 and 320 nm. When Eu$(TFA)_3$/Tb$(TFA)_3$ = 3:7, the white light phenomenon of the film is the strongest and the fluorescence characteristics are the best.

3. CONCLUSIONS

In summary, we successfully synthesized MMA monomer-functionalized CQDs and introduced unsaturated lanthanide complexes to obtain the dual-emission fluorescent composite material FCQDs-Ln$(TFA)_3$ (Ln = Eu, Tb). Both CQDs and lanthanide complexes have been combined in the PMMA matrix via chemical and physical interactions. A series of white fluorescent polymer films FCQDs-(Eu:Tb)$(TFA)_3$/PMMA with good dispersion and transparency were obtained by adjusting the ratio of lanthanide complexes Eu$(TFA)_3$ and Tb$(TFA)_3$ and characterized in detail. The intense white emission (CIE coordinate located at (0.36, 0.35)) can be observed with the optimum molar ratio (Eu/Tb = 3:7) when excited with a 320 nm laser. Most interestingly, the results revealed that FCQDs-Tb$(TFA)_3$ can be developed as a highly selective and sensitive luminescence probe for the detection of Fe^{3+} (LOD, 0.158 μM) through the fluorescence quenching of Tb^{3+} and CQDs. Moreover, FCQDs-Tb$(TFA)_3$ also realized the ratiometric detection in a wide pH range and displayed the strongest fluorescence emission in a neutral aqueous solution. Hence, the present study demonstrated that FCQDs-Tb-$(TFA)_3$ can be applied as a practical and multiresponse fluorescence probe with potential significance in environmental areas. This study provides a new idea and method for the research direction of functionalized carbon quantum dots

4. EXPERIMENTAL SECTION

4.1. Materials and Instruments. 1,2-Ethylenediamine (99%) was obtained from Sinopharm Chemical Reagent Co., Ltd. (Shanghai, China). Acrylic acid (99%), glycidyl methacrylate (GMA, 97%), 2,2′-azodiisobutyronitrile (AIBN, 99%) and methyl methacrylate (MMA, 99%), and all other reagents purchased from Aladdin Industrial Corporation

https://doi.org/10.1021/acsomega.1c01745
ACS Omega 2021, 6, 14629−14638

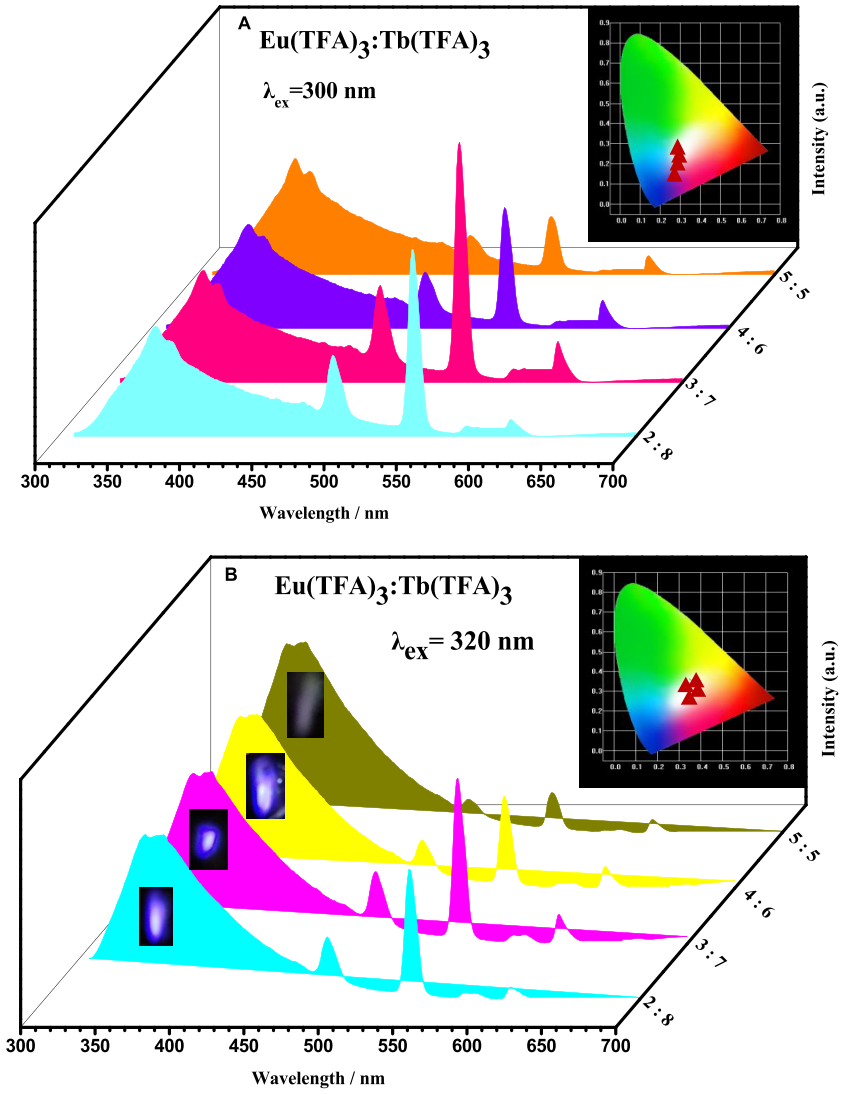

Figure 9. Emission spectra of FCQDs-(Eu:Tb)$(TFA)_3$/PMMA under excitation wavelengths of λ_{ex} = 300 nm (A) and λ_{ex} = 320 nm (B) with the corresponding CIE chromaticity diagram.

(Shanghai, China) were used directly in the as-received condition without further purification. PMMA (M_w = 43 982) used in this work was supplied by Alfa Aesar (Shanghai, China). Photoluminescence (PL) emission spectra were performed on an RF-5301 PC spectrophotometer with a 450W xenon lamp as the excitation source. FTIR spectra were measured on a Nexus 912 AO446 spectrophotometer in the range of 4000−400 cm^{-1}. ^1H NMR spectra of the samples were measured with an Ascend 400 spectrometer with D_2O and deuterated chloroform as solvents. The morphology and microstructure of the CQDs were determined by high-resolution transmission electron microscopy (HRTEM) on a Philips Tecnai G2 F30 microscope with an accelerating voltage of 200 kV. UV−vis absorption spectra were measured on a UV−vis spectrophotometer Lambda 750. X-ray photoelectric spectrometry (XPS) was performed on a PHI 5000 VersaProbe to reveal the interaction between the elements of the CQDs.

4.2. Synthesis of Carbon Quantum Dots (CQDs) and Polymerizable Carbon Quantum Dots (PCQDs). CQDs enriched with amine surface groups were prepared in a typical hydrothermal synthesis procedure using acrylic acid and 1,2-ethanediamine as the carbon source and surface passivation agent, respectively.[23,43] 1,2-Ethanediamine (2.68 mL, 40 mmol) and acrylic acid (2.75 mL, 40 mmol) were added to 35 mL of deionized water to form a transparent solution. The mixed solution was transferred into a 50 mL PPL-lined stainless-steel autoclave after the reaction was carried out at 160 °C for 6 h. When cooled down to room temperature, 20 mL of water was added to dissolve the formed yellow CQDs. The solution was dialyzed for 2 days in a dialysis bag (MWCO 1000), and the water was changed every 6 h. Finally, dry CQDs were obtained via lyophilization of the remaining water solution.

The polymerizable carbon quantum dots (PCQDs) were synthesized via a vinylation agent, glycidyl methacrylate (GMA), which reacted with amine groups on the CQDs' surface (Scheme 1). Dry CQDs (1.5 g) and GMA (10 mL) were dissolved in 20 mL of water and stirred for 24 h at 30 °C. Next, the oil phase of the solution was removed by a separating funnel, and the unreacted GMA molecules were removed by washing the water phase using *n*-hexane. Finally, the dry PCQDs were received by lyophilization of the remaining water solution. Scheme 1 shows the synthesis procedure and the surface modification reaction.

https://doi.org/10.1021/acsomega.1c01745
ACS Omega 2021, 6, 14629−14638

4.3. Synthesis of the Methyl Methacrylate-Functionalized CQDs (FCQDs). The functionalized CQDs (FCQDs) were prepared by radical polymerization. Typically, 980 mg of methacrylate (MMA) monomers and 20 mg of PCQDs were dissolved in 25 mL of *N*,*N*-dimethylformamide (DMF). Then, oxygen was removed with N_2 bubbling for 1 h under magnetic stirring. Next, the reaction system was heated to 80 °C, and immediately after preheating for 5 min, 10 mg of azodiisobutyronitrile (AIBN) was added to initiate polymerization and continued to react for 12 h at 80 °C, and then the solution was precipitated by 200 mL of water, filtered, and washed by water several times. Finally, FCQDs were dried under vacuum at 50 °C overnight.

4.4. Preparation of Lanthanide-Modified CQDs (FCQDs-Ln(TFA)$_3$). FCQDs (70 mg) and Ln(TFA)$_3$ (Ln = Eu, Tb; TFA = trifluoroacetylacetone) (1 mmol) were dissolved in 20 mL of absolute ethanol. The mixed solution was kept at 60 °C for 5 h. Finally, the reaction solution was cooled down with ice water and then the precipitate was collected by filtration and dried at 50 °C overnight.

4.5. Preparation of the Polymer Thin Film FCQDs-(Eu:Tb)(TFA)$_3$/PMMA. The PMMA powder (300 mg) was dissolved in 3 mL of dichloromethane (CH_2Cl_2), followed by the addition of the as-synthesized FCQDs (3 mg) and different ratios of complex solutions. We prepared a series of films by fixing the contents of the CQDs (3 mg) while varying the ratio of Eu(TFA)$_3$/Tb(TFA)$_3$ and finally gained a white luminescent film, as shown in Table 1. The resulting mixed solution was ultrasonically dispersed and stirred at room temperature for 30 min, poured into a glass dish, and placed in an oven to form a film at 30 °C.

4.6. Fluorescence Detection of Metal Cations. The FCQDs-Tb(TFA)$_3$ powder (3.0 mg) was dissolved in the aqueous solutions of different cations (Pb^{2+}, Cd^{2+}, Mg^{2+}, Zn^{2+}, Co^{2+}, Ni^{2+}, K^+, Mn^{2+}, Cu^{2+}, Ca^{2+}, Zn^{2+}, Co^{2+}, Ni^{2+}, K^+, Mn^{2+}, Cu^{2+}, Ca^{2+}, Fe^{2+}, and Fe^{3+}). Then, the mixtures were dispersed by an ultrasound system for about 30 min and placed in a fluorescence spectrophotometer to detect the change in fluorescence intensity.

4.7. Photoluminescence Stability Experiment. Three milligrams of the FCQDs-Tb(TFA)$_3$ powder was simply immersed into different pH solutions (3 mL). Then, the mixtures were dispersed for about 30 min by an ultrasound system, and fluorescence measurements were performed. Then, the mixture was dispersed through the ultrasonic system for about 30 min, and the fluorescence spectra were recorded when the excitation wavelength was 320 nm.

■ ASSOCIATED CONTENT

Supporting Information

The Supporting Information is available free of charge at https://pubs.acs.org/doi/10.1021/acsomega.1c01745.

XPS, FTIR, ^{1}H NMR, and UV−vis spectra of CQDs, PCQDs, and FCQDs; PL emission spectrum of FCQDs-Tb(TFA)$_3$ after 1 week; PL Intensity changes with pH; UV−vis spectra of Tb(TFA)$_3$ and FCQDs-(Eu:Tb)(TFA)$_3$/PMMA; and amount of each component in the film preparation process (PDF)

■ AUTHOR INFORMATION

Corresponding Author

Ying Li − *School of Materials Science & Engineering, University of Shanghai for Science and Technology, Shanghai 200093, P. R. China;* orcid.org/0000-0002-5159-5097; Email: liying@usst.edu.cn

Authors

Ya-Qi Wang − *School of Materials Science & Engineering, University of Shanghai for Science and Technology, Shanghai 200093, P. R. China*

Dan Liu − *School of Materials Science & Engineering, University of Shanghai for Science and Technology, Shanghai 200093, P. R. China*

Yu Gao − *School of Materials Science & Engineering, University of Shanghai for Science and Technology, Shanghai 200093, P. R. China*

Sai-Nan Wang − *School of Materials Science & Engineering, University of Shanghai for Science and Technology, Shanghai 200093, P. R. China*

Hanxun Qiu − *School of Materials Science & Engineering, University of Shanghai for Science and Technology, Shanghai 200093, P. R. China*

Complete contact information is available at: https://pubs.acs.org/10.1021/acsomega.1c01745

Notes

The authors declare no competing financial interest.

■ ACKNOWLEDGMENTS

This work was supported by the National Natural Science Foundation of China (21101107 and 51173107), the State Key Laboratory of Pollution Control and Resource Reuse Foundation (No. PCRRF19017), and the Staff Members of the Electron Microscopy System at the National Facility for Protein Science in Shanghai (NFPS, Zhangjiang Lab).

■ REFERENCES

(1) Li, D.; Jing, P.; Sun, L.; An, Y.; Shan, X.; Lu, X.; Zhou, D.; Han, D.; Shen, D.; Zhai, Y.; Qu, S.; Zboril, R.; Rogach, A. L. Near-Infrared Excitation/Emission and Multiphoton-Induced Fluorescence of Carbon Dots. *Adv. Mater.* **2018**, *30*, No. 1705913.

(2) Li, D.; Han, D.; Qu, S. N.; Liu, L.; Jing, P. T.; Zhou, D.; Ji, W. Y.; Wang, X. Y.; Zhang, T. F.; Shen, D. Z. Supra-(carbon nanodots) with a strong visible to near-infrared absorption band and efficient photothermal conversion. *Light: Sci. Appl.* **2016**, *5*, No. e16120.

(3) Guo, L.; Ge, J.; Liu, W.; Niu, G.; Jia, Q.; Wang, H.; Wang, P. Tunable multicolor carbon dots prepared from well-defined polythiophene derivatives and their emission mechanism. *Nanoscale* **2016**, *8*, 729−34.

(4) Mondal, T. K.; Ghorai, U. K.; Saha, S. K. Dual-Emissive Carbon Quantum Dot-Tb Nanocomposite as a Fluorescent Indicator for a Highly Selective Visual Detection of Hg (II) in Water. *ACS Omega* **2018**, *3*, 11439−11446.

(5) Zhou, Y.; Yang, S.; Fan, D.; Reilly, J.; Zhang, H.; Yao, W.; Huang, J. Carbon Quantum Dot/TiO_2 Nanohybrids: Efficient Photocatalysts for Hydrogen Generation via Intimate Contact and Efficient Charge Separation. *ACS Appl. Nano. Mater.* **2019**, *2*, 1027−1032.

(6) Shankar, S. S.; Shereema, R. M.; Ramachandran, V.; Sruthi, T. V.; Kumar, V. B. S.; Rakhi, R. B. Carbon Quantum Dot-Modified Carbon Paste Electrode-Based Sensor for Selective and Sensitive Determination of Adrenaline. *ACS Omega* **2019**, *4*, 7903−7910.

(7) Zhu, S.; Meng, Q.; Wang, L.; Zhang, J.; Song, Y.; Jin, H.; Zhang, K.; Sun, H.; Wang, H.; Yang, B. Highly photoluminescent carbon dots

for multicolor patterning, sensors, and bioimaging. *Angew. Chem., Int. Ed.* **2013**, *52*, 3953−7.
(8) Tang, J.; Zhang, Y.; Kong, B.; Wang, Y.; Da, P.; Li, J.; Elzatahry, A. A.; Zhao, D.; Gong, X.; Zheng, G. Solar-driven photoelectrochemical probing of nanodot/nanowire/cell interface. *Nano. Lett.* **2014**, *14*, 2702−8.
(9) Prasath, A.; Athika, M.; Duraisamy, E.; Selva Sharma, A.; Sankar Devi, V.; Elumalai, P. Carbon Quantum Dot-Anchored Bismuth Oxide Composites as Potential Electrode for Lithium-Ion Battery and Supercapacitor Applications. *ACS Omega* **2019**, *4*, 4943−4954.
(10) Yuan, F.; Wang, Z.; Li, X.; Li, Y.; Tan, Z.; Fan, L.; Yang, S. Bright Multicolor Bandgap Fluorescent Carbon Quantum Dots for Electroluminescent Light-Emitting Diodes. *Adv. Mater.* **2017**, *29*, No. 1604436.
(11) Yang, Y.; Lin, X.; Li, W.; Ou, J.; Yuan, Z.; Xie, F.; Hong, W.; Yu, D.; Ma, Y.; Chi, Z.; Chen, X. One-Pot Large-Scale Synthesis of Carbon Quantum Dots: Efficient Cathode Interlayers for Polymer Solar Cells. *ACS Appl. Mater. Interfaces* **2017**, *9*, 14953−14959.
(12) Li, L.; Zhu, X. Enhanced Photocatalytic Hydrogen Evolution of Carbon Quantum Dot Modified 1D Protonated Nanorods of Graphitic Carbon Nitride. *ACS Appl. Nano. Mater.* **2018**, *1*, 5337−5344.
(13) Chizhik, A. M.; Stein, S.; Dekaliuk, M. O.; Battle, C.; Li, W.; Huss, A.; Platen, M.; Schaap, I. A.; Gregor, I.; Demchenko, A. P.; Schmidt, C. F.; Enderlein, J.; Chizhik, A. I. Super-Resolution Optical Fluctuation Bio-Imaging with Dual-Color Carbon Nanodots. *Nano Lett.* **2016**, *16*, 237−42.
(14) Shi, Y.; Pan, Y.; Zhong, J.; Yang, J.; Zheng, J.; Cheng, J.; Song, R.; Yi, C. Facile synthesis of gadolinium (III) chelates functionalized carbon quantum dots for fluorescence and magnetic resonance dual-modal bioimaging. *Carbon* **2015**, *93*, 742−750.
(15) Hua, X. W.; Bao, Y. W.; Zeng, J.; Wu, F. G. Ultrasmall All-In-One Nanodots Formed via Carbon Dot-Mediated and Albumin-Based Synthesis: Multimodal Imaging-Guided and Mild Laser-Enhanced Cancer Therapy. *ACS Appl. Mater. Interfaces* **2018**, *10*, 42077−42087.
(16) Qu, S.; Zhou, D.; Li, D.; Ji, W.; Jing, P.; Han, D.; Liu, L.; Zeng, H.; Shen, D. Toward Efficient Orange Emissive Carbon Nanodots through Conjugated sp^2 -Domain Controlling and Surface Charges Engineering. *Adv. Mater* **2016**, *28*, 3516−21.
(17) Wang, H.; Sun, C.; Chen, X.; Zhang, Y.; Colvin, V. L.; Rice, Q.; Seo, J.; Feng, S.; Wang, S.; Yu, W. W. Excitation wavelength independent visible color emission of carbon dots. *Nanoscale* **2017**, *9*, 1909−1915.
(18) Cayuela, A.; Soriano, M. L.; Carrillo-Carrión, C.; Valcárcel, M. Semiconductor and carbon-based fluorescent nanodots: the need for consistency. *Chem. Commun.* **2016**, *52*, 1311−1326.
(19) Zhou, J.; Zhou, H.; Tang, J.; Deng, S.; Yan, F.; Li, W.; Qu, M. Carbon dots doped with heteroatoms for fluorescent bioimaging: a review. *Microchimi. Acta* **2017**, *184*, 343−368.
(20) Wang, Z.; Xu, C.; Lu, Y.; Chen, X.; Yuan, H.; Wei, G.; Ye, G.; Chen, J. Fluorescence sensor array based on amino acid derived carbon dots for pattern-based detection of toxic metal ions. *Sens. Actuators, B* **2017**, *241*, 1324−1330.
(21) Kim, S.; Hwang, S. W.; Kim, M. K.; Shin, D. Y.; Shin, D. H.; Kim, C. O.; Yang, S. B.; Park, J. H.; Hwang, E.; Choi, S. H.; Ko, G.; Sim, S.; Sone, C.; Choi, H. J.; Bae, S.; Hong, B. H. Anomalous Behaviors of Visible Luminescence from Graphene Quantum Dots: Interplay between Size and Shape. *ACS Nano* **2012**, *6*, 8203−8208.
(22) Wang, X.; Wang, D.; Guo, Y.; Yang, C.; Iqbal, A.; Liu, W.; Qin, W.; Yan, D.; Guo, H. Imidazole derivative-functionalized carbon dots: using as a fluorescent probe for detecting water and imaging of live cells. *Dalton Trans.* **2015**, *44*, 5547−54.
(23) Ding, H.; Wei, J. S.; Zhong, N.; Gao, Q. Y.; Xiong, H. M. Highly Efficient Red-Emitting Carbon Dots with Gram-Scale Yield for Bioimaging. *Langmuir* **2017**, *33*, 12635−12642.
(24) Chen, B.; Feng, J. White-Light-Emitting Polymer Composite Film Based on Carbon Dots and Lanthanide Complexes. *J. Phys. Chem. C* **2015**, *119*, 7865−7872.
(25) Wang, Z.; Yuan, F.; Li, X.; Li, Y.; Zhong, H.; Fan, L.; Yang, S. 53% Efficient Red Emissive Carbon Quantum Dots for High Color Rendering and Stable Warm White-Light-Emitting Diodes. *Adv. Mater* **2017**, *29*, No. 1702910.
(26) Liu, J.; Ge, X.; Sun, L.; Wei, R.; Liu, J.; Shi, L. Light modulation (vis-NIR region) based on lanthanide complex-functionalized carbon dots. *RSC Adv.* **2016**, *6*, 47427−47433.
(27) Wei, J-H.; Yi, J-W.; Han, M-L.; Li, B.; Liu, S.; Wu, Y-P.; Ma, L-F.; Li, D-S. A new water-stable terbium (III)-organic framework as a chemosensor for inorganic ions, nitro compounds and antibiotics in aqueous solutions. *Chem. Asian J.* **2019**, *14*, 3694−3704.
(28) Qin, Z.-S.; Dong, W.-W.; Zhao, J.; Wu, Y.-P.; Zhang, Q.-C.; Li, D.-S. A water-stable Tb(III)-based metal−organic gel(MOG) for detection of antibiotics and explosives. *Inorg. Chem. Front.* **2018**, *5*, 120−127.
(29) Arul, V.; Edison, T. N.; Lee, Y. R.; Sethuraman, M. G. Biological and catalytic applications of green synthesized fluorescent N-doped carbon dots using Hylocereus undatus. *J. Photochem. Photobiol., B* **2017**, *168*, 142−148.
(30) Duan, T.-W.; Yan, B. Hybrids based on lanthanide ions activated yttrium metal−organic frameworks: functional assembly, polymer film preparation and luminescence tuning. *J. Mater. Chem. C* **2014**, *2*, 5098−5104.
(31) Wu, J. X.; Yan, B. A dual-emission probe to detect moisture and water in organic solvents based on green-Tb^{3+} post-coordinated metal-organic frameworks with red carbon dots. *Dalton Trans.* **2017**, *46*, 7098−7105.
(32) Zhong, D.; Yang, K.; Wang, Y.; Yang, X. Dual-channel sensing strategy based on gold nanoparticles cooperating with carbon dots and hairpin structure for assaying RNA and DNA. *Talanta* **2017**, *175*, 217−223.
(33) Wu, J.; Hou, Y.; Wang, P.; Wang, Z.; Li, Y.; Wang, S.; Yang, M. Detection of lysozyme with aptasensor based on fluorescence resonance energy transfer from carbon dots to graphene oxide. *Luminescence* **2016**, *31*, 1207−1212.
(34) Cheng, W.; Pan, J.; Yang, J.; Zheng, Z.; Lu, F.; Chen, Y.; Gao, W. A photoelectrochemical aptasensor for thrombin based on the use of carbon quantum dot-sensitized TiO_2 and visible-light photoelectrochemical activity. *Mikrochim. Acta* **2018**, *185*, No. 263.
(35) Liu, Y.; Zhao, Y.; Fan, Q.; Khan, M. S.; Li, X.; Zhang, Y.; Ma, H.; Wei, Q. Aptamer based electro chemiluminescent thrombin assay using carbon dots anchored onto silver-decorated polydopamine nanospheres. *Mikrochim. Acta* **2018**, *185*, No. 85.
(36) You, X.; Lin, W.; Wu, H.; Dong, Y.; Chi, Y. Carbon dot capped gold nanoflowers for electro chemiluminescent aptasensor of thrombin. *Carbon* **2018**, *127*, 653−657.
(37) Chen, B. B.; Liu, M. L.; Zhan, L.; Li, C. M.; Huang, C. Z. Terbium (III) modified fluorescent carbon dots for highly selective and sensitive ratiometry of stringent. *Anal. Chem.* **2018**, *90*, 4003−4009.
(38) Chen, B. B.; Liu, Z. X.; Zou, H. Y.; Huang, C. Z. Highly selective detection of 2,4,6-trinitrophenol by using newly developed terbium-doped blue carbon dots. *Analyst* **2016**, *141*, 2676−81.
(39) Chen, H.; Xie, Y.; Kirillov, A. M.; Liu, L.; Yu, M.; Liu, W.; Tang, Y. A ratiometric fluorescent nanoprobe based on terbium functionalized carbon dots for highly sensitive detection of an anthrax biomarker. *Chem. Commun.* **2015**, *51*, 5036−5039.
(40) Xu, X.-Y.; Yan, B. Fabrication and application of a ratiometric and colorimetric fluorescent probe for Hg^{2+} based on dual-emissive metal−organic framework hybrids with carbon dots and Eu^{3+}. *J. Mater. Chem. C* **2016**, *4*, 1543−1549.
(41) Ren, Z.; Liu, X.; Chu, H.; Yu, H.; Xu, Y.; Zheng, W.; Lei, W.; Chen, P.; Li, J.; Li, C. Carbon quantum dots decorated $MoSe_2$ photocatalyst for Cr (VI) reduction in the UV−vis-NIR photon energy range. *J. Colloid Interface Sci.* **2017**, *488*, 190−195.
(42) Qu, S.; Chen, H.; Zheng, X.; Cao, J.; Liu, X. Ratiometric fluorescent nanosensor based on water soluble carbon nanodots with multiple sensing capacities. *Nanoscale* **2013**, *5*, 5514−8.

https://doi.org/10.1021/acsomega.1c01745
ACS Omega 2021, 6, 14629−14638

(43) Zhang, P.; Li, W.; Zhai, X.; Liu, C.; Dai, L.; Liu, W. A facile and versatile approach to biocompatible "fluorescent polymers" from polymerizable carbon nanodots. *Chem. Commun.* **2012**, *48*, 10431−1043.
(44) Zhao, A.; Chen, Z.; Zhao, C.; Gao, N.; Ren, J.; Qu, X. Recent advances in bioapplications of C-dots. *Carbon* **2015**, *85*, 309−327.
(45) Xu, X. Y.; Yan, B. Eu (III)-functionalized MIL-124 as fluorescent probe for highly selectively sensing ions and organic small molecules especially for Fe (III) and Fe (II). *ACS Appl. Mater. Interfaces* **2015**, *7*, 721−9.
(46) Tammina, S. K.; Yang, D.; Li, X.; Koppala, S.; Yang, Y. High photoluminescent nitrogen and zinc doped carbon dots for sensing Fe^{3+} ions and temperature. *Spectrochim. Acta, Part A* **2019**, *222*, No. 117141.
(47) Huxley, A. J. M.; Rademacher, J. T.; Rice, T. E.; Silva, A. P.; Gunaratne, H. Q. N.; Gunnlaugsson, T. *Higher Generation Luminescent Pet (Photoinduced Electron Transfer) Sensors*; Springer, 1997; pp 143−157.
(48) Batir, G. G.; Gedikli, S.; Arik, M. Pyronin b-graphene oxide-based turn-on fluorescent sensors for Fe^{3+} in an aqueous medium: synthesis and living cell application. *ChemistrySelect* **2017**, *2*, 10889−10894.
(49) Gao, X.; Zhou, X.; Ma, Y.; Qian, T.; Wang, C.; Chu, F. Facile and cost-effective preparation of carbon quantum dots for Fe^{3+} ion and ascorbic acid detection in living cells based on the "on-off-on" fluorescence principle. *Appl. Surf. Sci.* **2019**, *469*, 911−916.
(50) Yu, A.; Tang, Y.; Li, K.; Gao, J.; Zheng, Y.; Zeng, Z. Tunable photoluminescence studies based on blue-emissive carbon dots and sequential determination of Fe (III) and pyrophosphate ions. *Spectrochim. Acta, Part A* **2019**, *222*, No. 117231.
(51) Naik, V. M.; Gunjal, D. B.; Gore, A. H.; Pawar, S. P.; Mahanwar, S. T.; Anbhule, P. V.; Kolekar, G. B. Quick and low cost synthesis of sulphur doped carbon dots by simple acidic carbonization of sucrose for the detection of $Fe3^{+}$ ions in highly acidic environment. *Diamond Relat. Mater.* **2018**, *88*, 262−268.
(52) Rao, L.; Tang, Y.; Li, Z.; Ding, X.; Liang, G.; Lu, H.; Yan, C.; Tang, K.; Yu, B. Efficient synthesis of highly fluorescent carbon dots by microreactor method and their application in Fe^{3+} ion detection. *Mater. Sci. Eng., C* **2017**, *81*, 213−223.
(53) Wu, F.; Yang, M.; Zhang, H.; Zhu, S.; Zhu, X.; Wang, K. Facile synthesis of sulfur-doped carbon quantum dots from vitamin B1 for highly selective detection of Fe^{3+} ion. *Opt. Mater.* **2018**, *77*, 258−263.
(54) Xu, Q.; Pu, P.; Zhao, J.; Dong, C.; Gao, C.; Chen, Y.; Chen, J.; Liu, Y.; Zhou, H. Preparation of highly photoluminescent sulfur-doped carbon dots for Fe(III) detection. *J. Mater. Chem. A* **2015**, *3*, 542−546.

https://doi.org/10.1021/acsomega.1c01745
ACS Omega 2021, 6, 14629−14638